Analysis of microporous membranes obtained from polypropylene films by stretching

Sadeghi, Farhad; Ajji, Abdellah; Carreau, Pierre J.

Publisher's version / Version de l'éditeur:
https://doi.org/10.1016/j.memsci.2007.01.023
Journal of Membrane Science, 292, 1-2, pp. 62-71, 2007-01-24

Available online at www.sciencedirect.com
ScienceDirect
Journal of Membrane Science 292 (2007) 62–71
journal of MEMBRANE SCIENCE
www.elsevier.com/locate/memsci

Analysis of microporous membranes obtained from polypropylene films by stretching

Farhad Sadeghi [a], Abdellah Ajji [b], Pierre J. Carreau [a,*]

[a] *Center for Applied Research on Polymers and Composites, CREPEC, Ecole Polytechnique, Montreal, Que., Canada*
[b] *CREPEC, Industrial Materials Institute, CNRC, Boucherville, Que., Canada*

Received 31 August 2006; received in revised form 5 January 2007; accepted 17 January 2007
Available online 24 January 2007

Abstract

Five different polypropylene resins were selected to develop microporous membranes through melt extrusion and stretching (cast film process). The effect of the polymer melt elongation properties on the row-nucleated lamellar crystallization was investigated. The arrangement and orientation of the crystalline and amorphous phases were examined by WAXD (wide angle X-ray diffraction) and FTIR (Fourier transform infrared) methods. The extrusion and cooling parameters were adjusted properly to obtain uniform precursor films with appropriate morphology. Annealing, cold and hot stretching were consequently employed to generate and enlarge the pores. It was found that molecular weight was the most important material factor that controlled the membrane structure. The role of annealing and stretching parameters was also investigated. The permeability to water vapor (under atmospheric condition) and nitrogen (under pressure) was measured. It was observed that the permeability increased with increasing pressure and went through a transition from Knudsen diffusion to Poiseuille flow.

Keywords: Membranes; Polypropylene; Stretching; Lamellar structure; Orientation

1. Introduction

Membranes are increasingly employed for separation processes. From energy and processing points of view, they are progressively competing with the conventional separation processes such as distillation. Polymers are among the best candidates for the development of membranes covering a broad range of applications from microfiltration to reverse osmosis.

There are several techniques used for the fabrication of membranes and most of them are based on solution casting followed by phase separation. Solvent contamination and costly solvent recovery are two drawbacks for solution casting, although some improvements have been made in the recent decade [1]. One technique, which is applicable to semicrystalline polymers, is based on the stretching of a thin film with a row nucleated lamellar structure [2]. In this case pores are created as a result of lamellae separation. This method is relatively less expensive and there is no solvent contamination, but the major disadvantage is the low tear resistance in machine direction, due to the highly oriented structure of the film.

The fabrication of membranes by stretching is carried out in three main consecutive stages: (1) production of the precursor film with a lamellar morphology, (2) annealing of the film to thicken the lamellae, and (3) stretching of the film at low temperature to create voids and then stretching at high temperature to enlarge the pores [2]. One of the main issues in this process is the generation of a proper initial row nucleated structure. The polymer type and applied extrusion conditions are key factors for this method [3]. These factors determine the orientation and position of crystal blocks. Annealing will, in turn, partially remove the defects in the crystalline phase. The defects could be disruption of chain folding in the blocks or plane slippage. Annealing also improves the long spacing (the total thickness of the crystalline and amorphous phases that is almost periodically repeated) and a more uniform lamellae thickness distribution is obtained [4]. Consequently cold and hot stretching steps determine the configuration and properties of the obtained membrane. The parameters that affect the crystalline structure of the precursor films can be classified into material and process categories. The molecular weight and

* Corresponding author. Tel.: +1 514 340 4711x4924.
E-mail address: pcarreau@polymtl.ca (P.J. Carreau).

0376-7388/$ – see front matter © 2007 Elsevier B.V. All rights reserved.
doi:10.1016/j.memsci.2007.01.023

molecular weight distribution of the resins are the main material parameters controlling the crystalline lamellae and amorphous structures.

In this work, different polypropylene (PP) resins have been selected to study the effect of molecular weight on the crystalline structure and membrane formation. High molecular weight resins possessing long chains are good candidates for the generation of a proper row nucleated lamellar since they form long fibrils (threads) that act as sites for lateral lamellae crystallization [5]. If the quantity of the long chains is large, the number of threads goes up and they get very close to each other and lamellae impingement happens quickly [6]. Longer fibrils also improve orientation by keeping a strong scaffold for later crystallization. In contrast, for a small amount of long chains, there will be less threads and the longer distance between them can cause lamellae twisting [5].

The extrusion and production of the precursor films is a delicate process since the samples should be produced under high draw ratio and cooling rates. Although the presence of long chains is important for drawability and the crystalline structure, a very large number of long chains can cause problems. For example, the stick-slip phenomenon [7] was observed for a high molecular weight PP studied in our preliminary tests. The presence of low molecular weight tail (short chains) is generally undesirable for the formation of a row nucleated structure since it affects adversely the chain relaxation, but it improves melt processability via a smoother extrusion [8,9]. Obtaining a very uniform film is a major concern since any non-uniformity and thickness variations cause irregularities in the stress distribution.

Yu [2] studied the development of high density polyethylene (HDPE) membranes. He used two grades of HDPE with identical M_n (number averaged molecular weight) but differing in molecular weight distribution. The resin with a broader molecular weight distribution showed more elongated fibrils. As a result of more fibrils, the precursor film possessed a larger modulus and better mechanical properties in comparison to the resin with the narrower molecular weight distribution. Yu [2] also showed that annealing under a slight tension (3% strain) was more effective for lamellae thickening. He observed a reduction in permeability with increasing cold draw ratio beyond 40%. The microporous structure was found to be more uniform for the resin of broader molecular weight distribution, and this was attributed to the larger inter-lamellar tie chain density or fibril nuclei. He also observed that annealing at 120 °C in comparison to 105 °C could significantly increase the long period of the film structure.

Johnson [6] studied the process for the production of microporous membranes from poly(4-methyl-1-pentene) (PMP), and polyoxymethylene (POM) by stretching. He used the Gurley number (time required for 10 mL of air to pass through 1 in.^{2} section of film at a constant pressure of 12.2 in. of H_2O) to examine the permeability of the membranes. Lower Gurley numbers correspond to higher permeability. For PMP, cold stretching decreased the Gurley number while for a normalized Gurley number (time/thickness) the minimum Gurley occurred around a stretching of 80%. Also, the cold stretching temperature was shown to be optimum around 70 °C. Rising the hot stretching temperature up to 160 °C decreased the Gurley number, while there would be a possibility for structure deformation at very high temperature. He concluded that the initial decrease of the Gurley number with increasing cold stretch temperature was the result of a greater mobility within the amorphous phase rather than of the crystal phase (the PMP glass transition is 35 °C).

Polypropylene is widely produced in different grades and structures and, in comparison to polyethylene, PP shows better thermal stability and mechanical properties. Hence, it could be a more suitable candidate for the fabrication of microporous membranes. Although this material is commercially used in membrane development, very few articles have been published on this topic [10]. In this work we have investigated the role of material properties and process parameters on the structure and performances of PP porous membranes obtained by stretching of films.

2. Experimental

2.1. Materials

The five different polypropylene grades used in this study and key characteristics are presented in Table 1. PDC1280 (PP12) is a general purpose grade and Pro-fax 6823 (PP05) possesses the lowest MFR (melt flow rate), hence, the highest molecular weight in the homo polypropylene list introduced by Basell. Pro-fax 814 (PPB) is a branched polypropylene with long chain branches (its molecular weight is unavailable). It was selected because of the effect of branched chains on the relaxation time of the molten polyolefin. In this paper, we refer to these materials as PP12, PP05 and PPB. PP4292E1 (PP20) and PP4612E2 (PP28) are ExxonMobil grades used for the production of oriented films. The manufacturer reports these two resins as homopolymers with bimodal molecular weight distributions. An FTIR test was carried out and no trace of ethylene was found in the absorption spectrum of both resins.

Table 1
Polypropylene grades used and key properties

Resin code	Company	MFR 230 °C/2.16 kg	Nomenclature in this paper	M_w (kg/mol) [3]
PDC1280	Basell	1.2	PP12	420.5
Pro-fax 6823	Basell	0.5	PP05	510.8
Pro-fax 814	Basell	2.8	PPB	n/a
PP4292E1	ExxonMobil	2.0	PP20	416.5
PP4612E2	ExxonMobil	2.8	PP28	350.3

2.2. Rheological characterization

The rheological behavior of the resins was determined using an ARES rheometer (Rheometric Scientific). Stress relaxation experiments were carried out for a large step strain. The extensional viscosity was measured via the new SER universal testing platform from Xpansion Instruments. The model used in our experiment was SER-HV-A01, which is a dual windup extensional rheometer and has been specifically designed for the ARES rheometer platform. It is capable of generating elongational rates up to $20\,s^{-1}$ under controlled temperature (up to 250 °C).

2.3. Film preparation

The films were prepared by cast film processing with a slit die at the temperature of 220 °C. To improve cooling, a fan was installed to supply air to the film surface right at the exit of the die. The key parameters were the fan speed, take-up roll speed and die temperature. We worked at the maximum speed of the fan and constant die temperature, so the only variable was the take-up speed. Since the extrudate velocity at the exit of the die was constant the take-up speed determined the draw ratio for the film production. For PP05 (the highest molecular weight resin), the cooling had to be reduced to 70% of the rate used for the other resins to obtain stable films.

2.4. Film and membrane characterization

Crystal orientation measurements were carried out using a Bruker AXS X-ray goniometer equipped with a Hi-STAR two-dimensional area detector. The generator was set up at 40 kV and 40 mA and the copper Cu K_a radiation ($\lambda = 1.542$ Å) was selected using a graphite crystal monochromator. The sample to detector distance was fixed at 8 cm. Prior to measurements, careful sample preparation was required to get the maximum diffraction intensity. This consisted in stacking several film layers in order to obtain the optimum total thickness of about 2.5 mm.

Tensile tests were performed using an Instron 5500R machine equipped with a chamber for running tests at high temperature. The procedure used was based on the D638-02a ASTM standard.

For FTIR measurements, infrared spectra were recorded on a Nicolet Magna 860 FTIR instrument from Thermo Electron Corp. (DTGS detector, resolution $4\,cm^{-1}$, accumulation of 128 scans). The beam was polarized by means of a Spectra-Tech zinc selenide wire grid polarizer from Thermo Electron Corp. The crystalline and amorphous orientations were measured based on the method that has been explained in detail in Ref. [3].

The DSC (differential scanning calorimetry) tests were carried out on a TA Instruments Q1000 for a heating rate of 20 °C/min.

Permeability of water vapor was measured via a MOCON PERMATRAN-W Model 101 K at room temperature. For nitrogen the flow of gas transmitted through the membrane was measured with a photo flowmeter (Optiflow520). The set-up for nitrogen permeability was built in our lab.

For porosimetry, the pore size distribution and porosity were evaluated using a mercury porosimeter (Pore Sizer 9320-Micromeritics).

3. Results and discussion

3.1. Extrusion and materials

Fig. 1 shows the stress–strain curves for the melts obtained from the extensional viscosity measurements at a temperature of 200 °C and an elongational rate of $5\,s^{-1}$. The strain rate was similar to the value applied to the molten extrudate at the exit of the die while for temperature we could not conduct the experiment at a higher temperature because of sagging of the samples. The decreases of the stress at high strain for the homopolymers are indicative of sample failure. As expected the largest molecular weight resin (PP05) exhibits the largest extensional properties among the homopolymers and its stress increases smoothly up to a strain value close to 3, which is slightly larger than for the general purpose grade (PP12). For the two bimodal resins, PP20 and PP28, the stress is increasing further up to a strain of 3.4. The behavior is totally different for PPB, which shows a rapidly ascending trend. This is the result of strain hardening, which occurs for a resin with long chain branches. While PPB shows a good melt strength, its lower molecular weight results in poor drawability [8] and also mechanical properties for the films. The linear viscoelastic properties of these resins can be found in Sadeghi et al. [3].

It should be noted that the effect of the extrudate temperature at the die exit is not trivial. A lower temperature will more likely preserve the initial state of polymer chains but it will affect the extrusion process. A lower die temperature also reduces the mobility of the chains to be extended at high draw ratios at the die exit and also influences the mobility of the shorter chains for secondary crystallization.

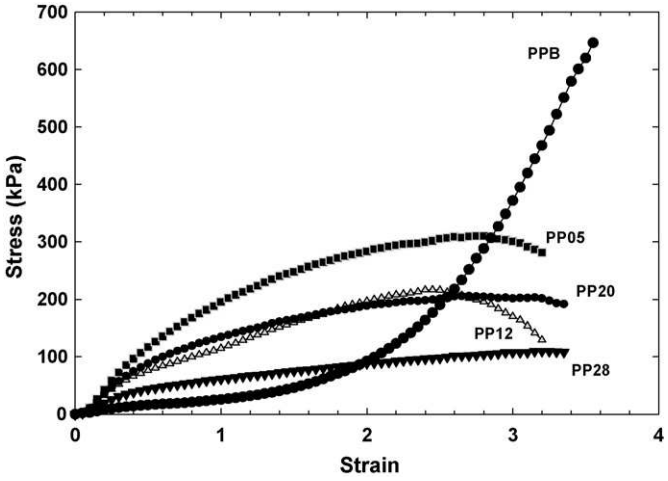

Fig. 1. Stress–strain obtained from the elongational tests at the elongational rate of $5\,s^{-1}$ and 200 °C.

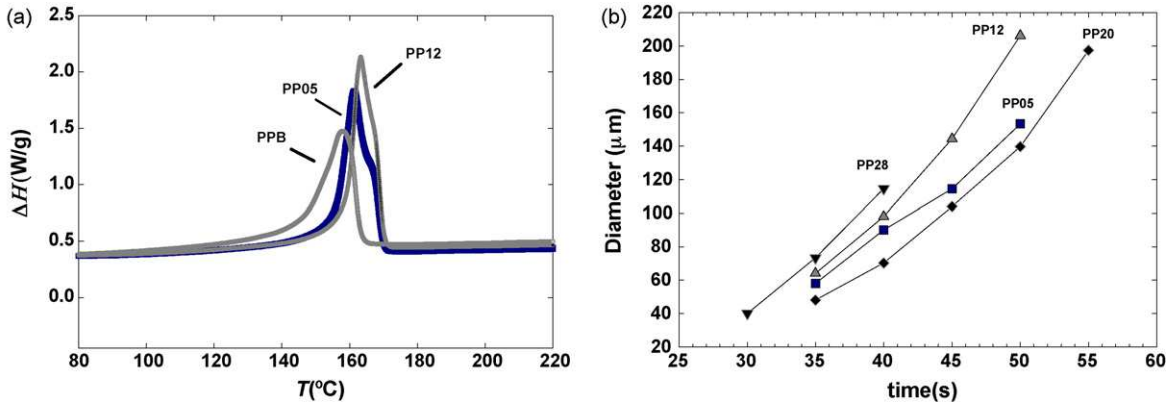

Fig. 2. (a) DSC of the PP films (heating rate of 20 °C/min) and (b) crystal growth vs. time (cooling rate of 20 °C/min).

3.2. Crystallization and solidification

The stress-induced crystallization is influenced, in addition to material parameters, by strain, strain rate and cooling conditions. These parameters control the lamellae structure such as crystal thickness, orientation and type of the crystals. DSC tests were performed on the precursor films prepared with a draw ratio of 65 and under maximum cooling rate (except for PP05 for which 70% cooling rate was used). The key results are presented in Fig. 2a. The DSC results for PP20 and PP28 were quite similar to those of PP05 and, hence, are not presented in Fig. 2a. Since the melting peaks of all samples (except PPB) did not change much, it was assumed that the lamellae thickness was of the same order. Hence, the major difference in the crystalline structure of the precursor film is thought to come from orientation of the crystal blocks and configuration of tie chains connecting crystal blocks (tie chain density, length and orientation). We believe that the film samples from a very high molecular weight resin possess a larger amount of strong threads, which makes lamellae separation difficult. We observe in Fig. 2a a slight shoulder at higher temperature for the film of PP05 (also for the films of PP20 and PP28 not shown). WAXD results (discussed later) revealed only one crystalline form (α) for the precursor films and no trace of β crystalline form could be observed. Since the resins are all considered homopolymers the shoulder peak can only be attributed to lamellae distribution (thinner and thicker lamellae).

Cooling is a critical controlling factor in the formation of precursor films [4]. Although very efficient cooling conditions are necessary to prevent chains relaxation at the die exit, rapid cooling might affect the secondary crystallization (lamellae growth). Therefore, there should be optimum cooling conditions to obtain the appropriate lamellae structure.

We did not have any mean to measure the crystal growth under stress, but we studied the spherulitic growth for these resins under quiescent crystallization conditions. Apparently, the stress conditions mostly affect the nucleation stage while the spherulitic growth proceeds through secondary crystallization (similar to lamellae growth) and is controlled by the cooling conditions. As it can be seen from Fig. 2b the spherulitic growth rate, given by the slope of the curves, is almost the same for the four resins. The results for PPB (long chain branched PP) are not shown in Fig. 2b because they showed a large amount of very tiny spherulites, smaller than the range of our measurement accuracy.

3.3. Annealing

Annealing is performed at a certain temperature that is the beginning of the mobility in the crystalline structure (T_α) [6]. This annealing removes the defects in the crystalline structure, thickens the lamellae and finally improves lamellae orientation and uniformity [11]. Although annealing usually takes place in a short time, its role is critical in membrane production. The three controlling factors are annealing time, annealing temperature and applied stress during annealing. Some authors found that a slight tension during annealing is effective [2], improving orientation, but in our case we did not observe any significant improvement. Annealing increases the long period (total thickness of the crystal and amorphous phases) [12]. It is estimated that much of the long period improvement is due to the increasing of the lamellae thickness. We observed that for polypropylene under quiescent annealing (in absence of stress) the efficient annealing time was 10 min at 140 °C and beyond that, the structure parameters remained constant. This has also been reported for PE films [2].

The annealing temperature is probably the most important factor here. It should be noted that increasing temperature to a high degree might deteriorate the initial lamellar crystalline structure through local partial melting and recrystallization. Fig. 3 compares the DSC results for annealed and non-annealed samples of a precursor PP28 film. A small peak is observed around 140 °C after annealing, as it has also been reported by other authors [13]. It can be observed that the area under the curves is also increased after annealing, which means an improvement in crystallinity. The position of the peak did not change significantly suggesting that the crystal thickness change was negligible. Annealing improved the orientation significantly as shown in Table 2 [3]. The same trend was observed for all other films. The improvement in crystal orientation after annealing has been addressed elsewhere [11]. Annealing provides a possibility for the lamellae to be rearranged in machine direction resulting

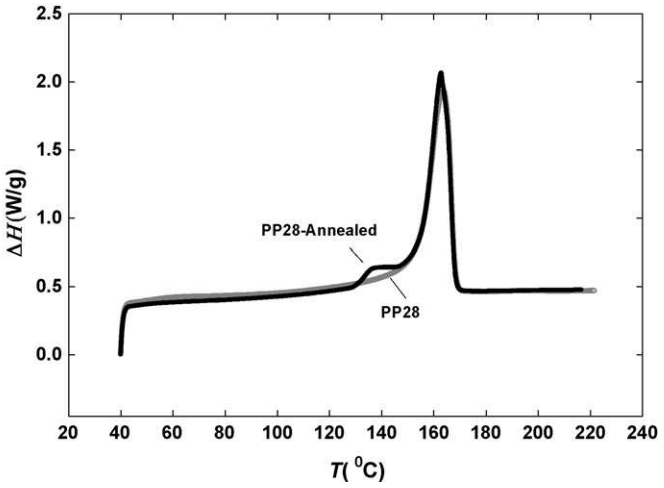

Fig. 3. DSC of the PP28 annealed and non-annealed samples (annealing time of 10 min at 140 °C; heating rate of 20 °C/min).

Table 2
Orientation of crystalline and amorphous phases

Resin	DDR	f_c	f_{av}	f_a
PP05[a]	65	0.710	0.517	0.381
PP05-An[b]	65	0.769	0.568	0.427
PP12	48	0.512	0.374	0.277
PP12-An	48	0.584	0.435	0.33
PP12-An-150 °C	48	0.667	0.498	0.379
PP12	65	0.623	0.448	0.325
PP12-An	65	0.721	0.534	0.402
PP12-half strain rate	65	0.608	0.439	0.319
PP20	65	0.556	0.390	0.272
PP20-An	65	0.698	0.522	0.398
PP28	65	0.484	0.348	0.259
PP28-An	65	0.569	0.424	0.328

[a] As it was mentioned there were more noticeable thickness variations for the PP05 precursor film. For this case the measurement was made for a sample taken from the middle of the film.
[b] Annealing was performed for 1 h and at 140 °C unless other conditions are mentioned.

in orientation improvement. Since tie chains are connecting the lamellae, rearrangement and improvement in the orientation of the lamellae would affect the tie chains as well. That could be an explanation for the rise in amorphous orientation. We did not anneal any PPB samples since the film could not be stretched for membrane development, probably due to its low molecular weight.

Wide angle X-ray diffraction measurements were carried out on the annealed samples. Fig. 4 shows the diffraction patterns for two PP films (high and low molecular weight PP samples). The first ring represents the 1 1 0 and the second one is the 0 4 0 crystalline plane. The normal to the 1 1 0 plane is the bisector of the *a*- and *b*-axes and 0 4 0 is along the normal of the *b*-axis of unit crystal cells, as shown in the sketch of Fig. 4(d). The arcs are sharper for PP05 (highest molecular weight resin) and more concentrated while no major difference is observed for the WAXD spectrum (intensity versus 2θ). With respect to the Scherrer equation [12] and the inverse dependency of the width of the half maximum of a peak on crystal thickness, a conclusion can be drawn that the lamellae thickness does not change at least along the *a*- and *b*-axes. Hence, it is assumed that the effect of molecular weight is more pronounced on the orientation of lamellae as it will be shown later.

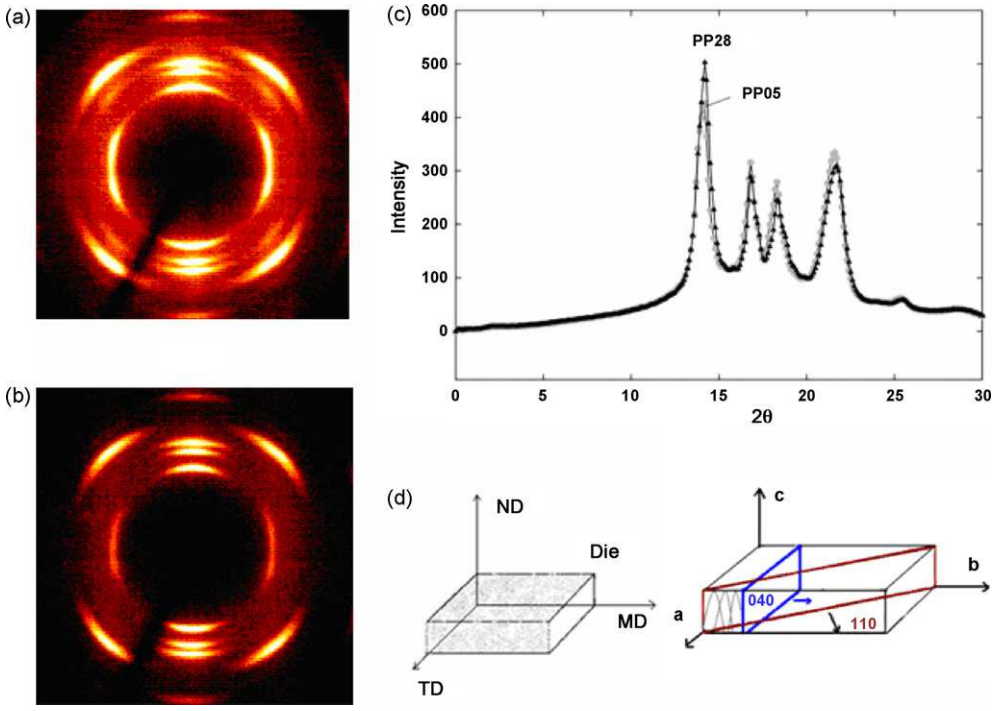

Fig. 4. WAXD patterns of the annealed precursor films (a) low and (b) high molecular weight resins with initial draw ratio of 65, (c) diffraction spectrum with integration throughout the circles and (d) the crystal planes with respect to fixed coordinates.

The orientation and position of the crystal blocks in the precursor films control the lamellae separation process, which results in pores formation. The orientation of the amorphous and crystalline phases (*c*-axis with respect to MD) of the samples has been measured by Fourier transform infrared spectroscopy and the results are presented in Table 2. The orientation function was calculated as [14]:

$$f_{i,\mathrm{MD}} = \frac{D-1}{D+2} \tag{1}$$

where D is the ratio of the absorbance in the machine (parallel) to that in the transverse (perpendicular) direction. For the orientation function of the crystal phase (*c*-axis with respect to MD), f_c, the band at 998 cm^{-1} is considered so D will be $(A_\parallel/A_\perp)_{998}$, where A is the absorbance. To measure the total orientation that includes both the crystalline and the amorphous phase orientations the band at 972 cm^{-1} was selected and f_{av} (average orientation) was calculated based on $(A_\parallel/A_\perp)_{972}$. The orientation of the amorphous phase, f_a, can be determined from these two values by

$$f_{\mathrm{av}} = X_c f_c + (1 - X_c) f_a \tag{2}$$

where X_c is the degree of crystallinity. We have shown that the *c*-axis crystal orientation measured by FTIR is in reasonable agreement with the values obtained from the WAXD results [3].

The processing conditions have also been listed in Table 2 along with the results for the orientations of the crystalline and amorphous phases. Annealing improves the amorphous orientation along the machine direction. This is likely due to the participation of disrupted amorphous chains (end chains) in the crystallization and also the partial motion of the crystal blocks, which results in a slight stretching of the tie chains along the lamellae thickness. The effect of temperature and strain rate is also shown in Table 2. The annealing temperature significantly improves orientation while reducing the strain rate applied at the die decreases the orientation for both the crystalline and amorphous phases.

3.4. Cold stretching

After annealing, the precursor films were stretched at room temperature for lamellae separation and pores creation. The tensile properties for tests carried out with a recovery response following an applied strain of 1 are presented in Fig. 5. The speed of stretching was 200 mm/min and the same speed was used in the recovery to return to the initial length. It should be noted that in our process for making membranes we usually considered a strain of 0.4 for cold stretching.

The recovery of the applied strain, which reflects the elasticity of the film, is controlled by factors such as crystal thickness, tie chain density and orientation. The whole process is governed by the stretching of two types of tie chains. Initially, the short tie chains are stretched out and are finally broken apart (end of the elastic region) resulting in pores creation [11]. However, at the end of this region the sample can recover most of the initial strain (if relaxed) because of the connection of long tie chains. After this point the stress is transferred to the long tie chains. The enlargement of the pores proceeds with stretching of the long tie chains. The stretched long tie chains could go then through crystallization in a later hot stretching step to form strong interconnected bridges [11]. As shown in Fig. 5, PP05 failed around a strain of 1 (the ultimate limit for the tie chain stretching). We believe this could be due to a larger amount of extended fibrils that strongly connect the lamellae together. High molecular weight chains promote orientation through the creation of long fibrils. On the other hand, long fibrils limit the mobility of the lamellae for separation in stretching. PP28 showed a maximum recovery in comparison with the other resins, which could be the result of less pores formation (lower structure damage) and also more flexibility in the lamellae motion. The use of a larger draw ratio in the precursor films, as shown in Fig. 5 by comparing results for PP12-48 and PP12-65, also improved the strain recovery. The improvement could be due to a higher orientation of the structure.

The annealed samples were cold stretched to 40% at 25 °C and heated up to 140 °C for 20 min for heat setting to fix the pore structure. Fig. 6 presents the SEM micrographs of the

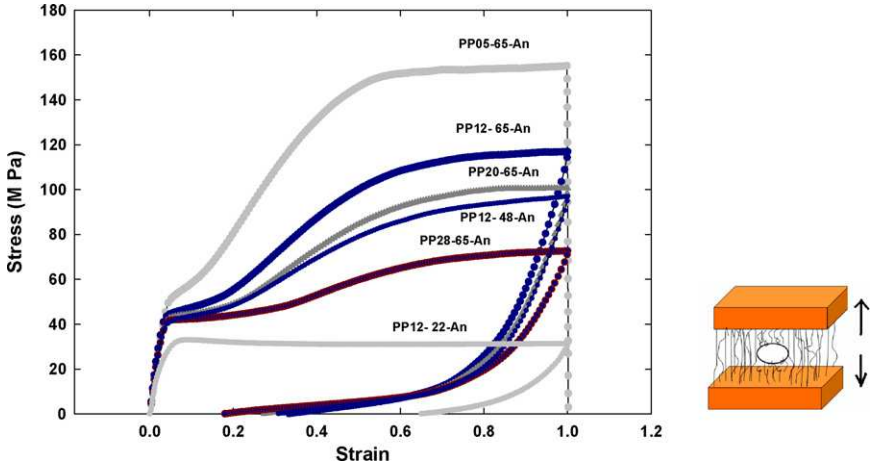

Fig. 5. Tensile properties of annealed samples; stretching and recovering were performed at a speed of 100 mm/min.

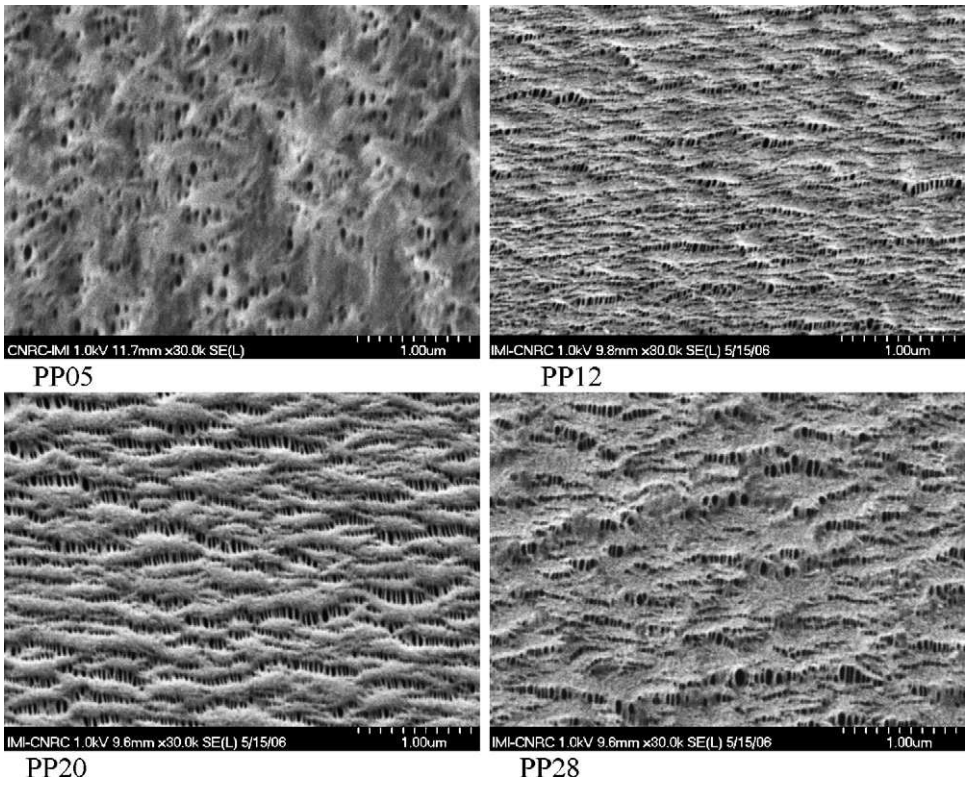

Fig. 6. SEM micrograph of the surface of PP (initial draw ratio of 56.5) samples cold stretched to 40% and heated up to 140 °C for 20 min for heat setting.

samples after cold stretching. It is clear that the pores size does not vary significantly from one resin to the others. However, there is a difference in the lamellae thickness. The pores are more uniformly distributed for PP20 and less uniform for PP05. As these images were taken from the surface, the important issue is the interconnection state between the pores along the thickness, which controls the permeability. In fact, interconnected pores determine the membrane performances. The effective factors in this case are the orientation of the crystal blocks and also the structure uniformity along the width of the film. Even though PP05 showed a good orientation of the crystal blocks, strong interconnection between the lamellae reduced mobility and hindered lamellae separation. Thickness variations (as a result of non-uniform cooling) along the width did not allow for a constant stress distribution over the cross-section.

3.5. Hot stretching

After cold stretching and formation of pores, samples that were not heat set were stretched again to 40% at an elevated temperature (140 °C) to enlarge the pores. For a constant hot stretch level it has been shown that the permeability is improved as the specific hot stretch temperature is increased [5]. Fig. 7 depicts the pore structure of two samples, for which the surface structures are shown in Fig. 6 after cold stretching. It seems that for PP20 the pores are a little larger. The pore diameter changed after hot stretching but not dramatically. We can consider an

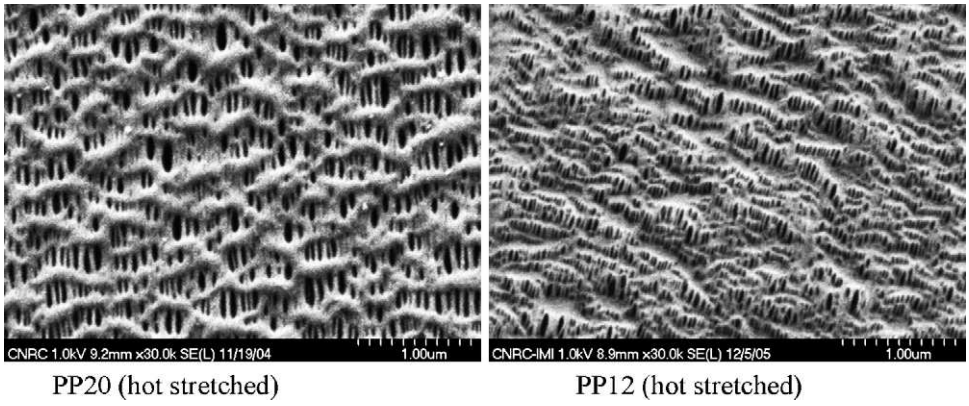

Fig. 7. SEM micrographs of the two hot stretched (40% at 140 °C) samples already presented in Fig. 6.

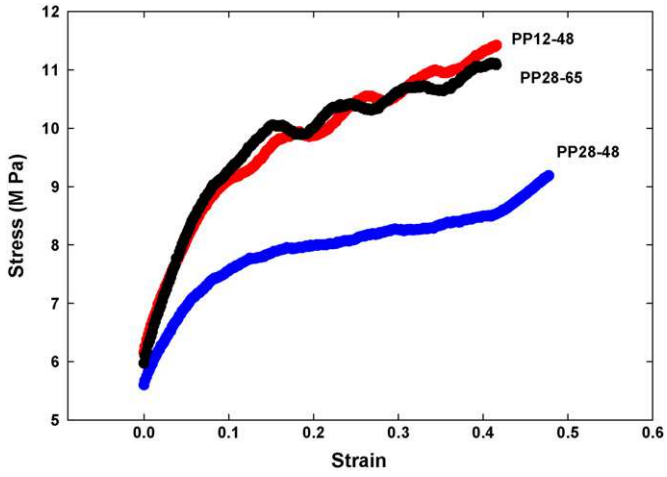

Fig. 8. Tensile properties for three samples at 140 °C.

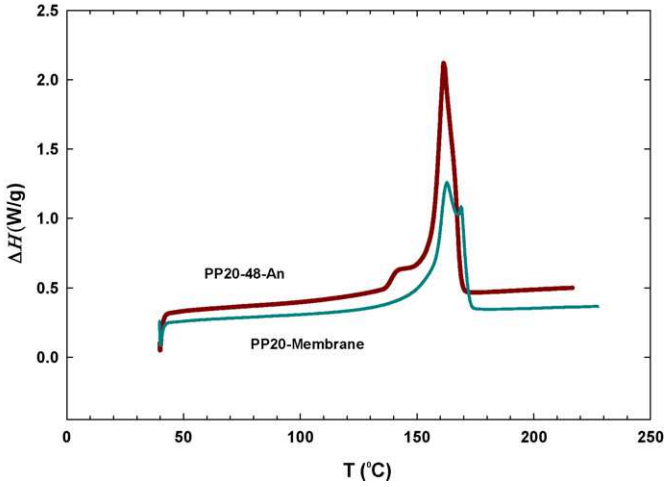

Fig. 9. DSC of the final PP20 membrane (with initial draw ratio of 48) compared with the annealed sample.

average of 120–200 nm for PP20, while for PP12 the pore size is smaller. However, comparing the pore sizes from micrographs should be done with caution. In fact the interconnection (created channels along the thickness) between the pores determines the effective pore diameter.

We believe that in the hot stretching stage, some lamellae are melted and recrystallized in the form of interconnected bridges. This is a complex process, but it is the most probable phenomenon that could happen as suggested by the observation of a decrease in the lamellae thickness along with creation of more interconnecting bridges. The unraveling of folded polymer chains and their complete reorientation have also been reported elsewhere [11]. On the other hand, some pores that are invisible after the cold stretching as initiated pores are enlarged during the hot stretching process. These phenomena could explain the increase in the number of pores during the hot stretching stage as well. Fig. 8 shows the stress consumption in the samples at 140 °C during an Instron tensile test (with a similar speed as applied during the hot stretching of the samples). The stress consumption increases with the initial draw ratio and the molecular weight. The stress at this stage is mostly spent: (i) to separate the lamellae to a larger extend and (ii) to stretch the tie chains with simultaneous crystallization of some of them, which increase the number of interconnected bridges. There is also a possibility for reorientation and motion of the crystal blocks in the stretching direction, which requires a larger share of the stress for the samples with lower orientation.

DSC of the produced membranes provides us with some information regarding the lamellae thickness distribution. Fig. 9 shows the DSC results for the final PP20 membrane compared with the previous annealed film. The evolution in the crystalline structure can be seen after final stretching. The two distinctive peaks suggest two types of lamellae distribution. It is assumed that one of these peaks corresponds to crystals of the interconnected bridges between the lamellae and the other reflects the lamellae crystals.

3.6. Permeability

Permeability of the produced membranes was evaluated by water vapor and nitrogen. Water vapor permeability was performed under atmospheric conditions (no pressure applied) and with cross-flow configuration while for nitrogen, a pressured system was used to monitor the flow rate versus pressure. Table 3 reports the water vapor permeability for the membranes. The permeability results are in accordance with the orientation results presented in Table 2 except for PP05. The lower permeability for PP05 could be due to two factors: first, there was a non-uniformity observed along the width of the precursor film as

Table 3
Permeability of the membranes prepared using different processing conditions

Resin	Conditions: DR = draw ratio; t = membrane thickness	Permeability at the end of cold stretching stage (g/m^2 day) (error: ±5%)	Permeability of final membranes (at the end of hot stretching) (g/m^2 day) (error: ±5%)
PP05	DR = 56.5, t = 24 μm, cooling = 70%[a]	2,200	12,000
PP12	DR = 56.5, t = 24 μm	12,700	23,800
PP20	DR = 56.5, t = 24 μm	14,100	21,000
PP28	DR = 56.5, t = 24 μm	8,700	17,750
PP20	$T_{\text{Cold stretching}}$ = 50 °C	[b]	25,050
PP12	DR = 65, t = 22 μm	[b]	29,800
PP12	DR = 65 produced under half strain rate, t = 22 μm	[b]	25,400

[a] As we mentioned previously for obtaining a stable and uniform sample we had to use 70% of the cooling (fan speed) used for the other resins.
[b] Not measured.

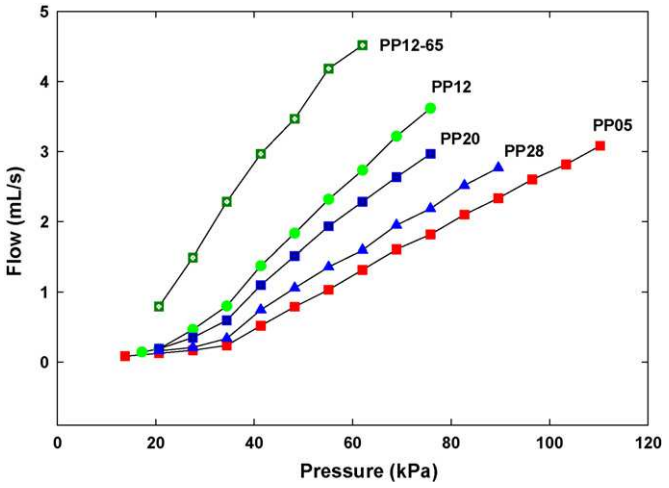

Fig. 10. Flow vs. applied pressure for nitrogen for the membranes produced with initial draw ratio of 56.5 (as presented in Table 3) and for one membrane prepared at a draw ratio of 65.

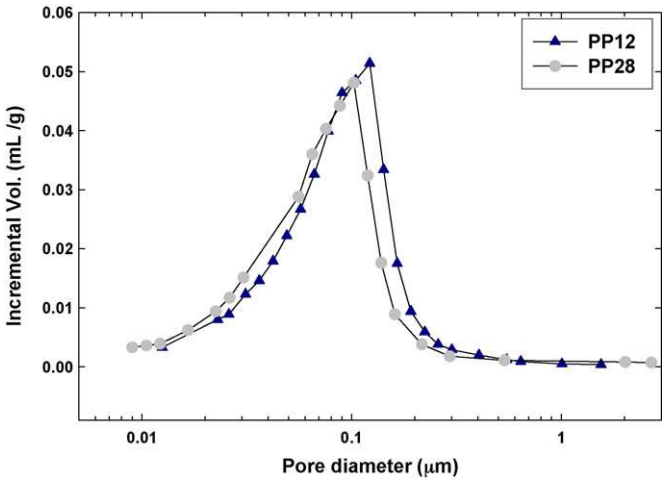

Fig. 11. Pore size distribution for two microporous PP12 and PP28 membranes, with initial precursor films prepared under a draw ratio equal to 56.5.

mentioned before, which disturbed the stress distribution and, second, the presence of a large number of long chains for this resin resulted in many long thick threads that did not lead to an easy lamellae separation. The SEM micrograph of this sample (Fig. 6) shows the non-uniformity of the pores distribution. It is observed for PP20 that increasing the cold temperature from 25 to 50 °C improves slightly the permeability. The PP12 sample obtained under a larger initial draw ratio shows a 25% increase in permeability whereas the PP12 sample prepared at a lower strain rate but under the same draw ratio of 65 (as mentioned in the extrusion section) shows a 18% drop in permeability. This is probably due to a weaker row nucleated lamellar structure, even though the orientation stays almost constant for the sample (Table 2).

Fig. 10 presents the permeability to N_2 under pressure of the membranes. The ranking of the membrane permeability to N_2 is the same as the ranking for the values to water vapor reported in Table 3. Two distinguishable regimes are observed, characterized by the difference in slope as a function of pressure: at low pressure, the behavior reflects the Knudsen diffusion process (no pressure effect) and at high pressure this is the Poiseuille flow regime (linear pressure effect) [15]. The transition between the Knudsen regime and Poiseuille flow occurs around a pressure of 0.35×10^5 Pa. The transition is less pronounced for the membranes with higher permeability. The higher permeability is a result of larger orientation that improves the interconnection between the pores. In the case of lower orientation the pore interconnection is weak and the porosity is decreased. However, the effect of thickness should also be considered here since both high orientation and smaller thickness intensify this effect.

3.7. Mercury porosimetry

The porosity and pore size distribution from mercury porosimetry are reported in Fig. 11 for two microporous PP12 and PP28 films, with initial precursor film draw ratio of 56.5. For PP12 (high permeability) a peak in the pore size distribution around 0.15 μm is observed while for PP28 (lower permeability), the whole curve shifts to lower values with a peak around 0.10 μm. The porosity was evaluated as 47 and 41% for PP12 and PP28 films, respectively. Although the SEM micrographs of the surface of PP12 and PP20 samples are quite different (see Fig. 7), their pore size distribution and porosity are about the same (results not shown for PP20). The intrusion volume of mercury is directly related to pore size and porosity for interconnected pores. Lower effective pore size for the resin with smaller molecular weight could be attributed to lower orientation resulting in less pore interconnection.

4. Conclusion

The process for developing microporous membranes covers several stages, which are precursor film production, annealing, cold and hot stretching. The molecular weight of the base resin seems to be one of the key parameters for predicting membrane performances provided that the proper extrusion process is employed. In this work, five different PP resins have been investigated. These resins of distinct molecular weights showed different melt behavior during stress relaxation as well as under uniaxial elongation. DSC results showed changes in lamellae distribution in each step starting from precursor films to membranes. The lamellae thickness did not show a large dependency on molecular weight while most impact of molecular weight was revealed on the orientation and connectivity of lamellae. The most effective parameter in annealing was temperature, which highly improved the crystal phase orientation, while it had a much weaker effect on the amorphous phase. It was found that cold stretching also initiated some pores, which might not be visible in cold stretched samples, but would appear in the hot stretching step.

The water vapor permeability of the membranes, which reflects the pore interconnection, depended on molecular weight and orientation in the samples. The permeability to N_2 under pressure showed two distinguishable regimes. A change from

Knudsen to Poiseuille flow was observed as the pressure was increased. The behavior of the samples with high orientation in the precursor films was mainly controlled by Poiseuille flow. The high permeability PP12 membrane had pores around 0.15 μm and porosity of 47% whereas the lower permeability PP28 membrane had smaller pores of 0.10 μm and porosity of 41%.

Acknowledgements

Financial support from NSERC (Natural Science and Engineering Research Council of Canada) and from FQRNT (Fonds Québécois de Recherche en Nature et Technologies) is gratefully acknowledged.

References

[1] M. Cheryan, Ultrafiltration and Microfiltration Handbook, 2nd ed., CRC Press LLC, Boca Raton, FL, 1998.
[2] T.H. Yu, PhD Thesis, Virginia Polytechnic Institute and State University, 1996.
[3] F. Sadeghi, A. Ajji, P.J. Carreau, Orientation analysis of row nucleated lamellar structure of polypropylene obtained from cast film, Polym. Eng. Sci., in press.
[4] H.D. Noether, I.L. Hay, Small-angle X-ray diffraction studies and morphology of microporous materials and their 'hard' elastic precursors, J. Appl. Cryst. 11 (1978) 546.
[5] F. Sadeghi, A. Ajji, P.J. Carreau, Study of polypropylene morphology obtained from blown and cast film processes: initial morphology requirements for making porous membrane by stretching, J. Plastic Film Sheeting 21 (2005) 199.
[6] M.B. Johnson, PhD Thesis, Virginia Polytechnic Institute and State University, September 2000.
[7] H. Münstedt, M. Schmidt, E. Wassner, Stick and slip phenomena during extrusion of polyethylene melts as investigated by laser-Doppler velocimetry, J. Rheol. 44 (2000) 413.
[8] M. Dupire, J. Michel, Polypropylene with high melt strength and drawability, US Patent 6,723,795 (2004).
[9] Z. Bashir, J.A. Odell, A. Keller, Stiff and strong polyethylene with shish kebab morphology by continuous melt extrusion, J. Mater. Sci. 21 (1986) 3993.
[10] J.J. Kim, T.S. Jang, Y.D. Kwon, U.Y. Kim, S.S. Kim, Structural study of microporous polypropylene hollow fiber membranes made by the melt-spinning and cold-stretching method, J. Membr. Sci. 93 (1994) 209.
[11] I.K. Park, H.D. Noether, Crystalline "hard" elastic materials, Colloid Polym. Sci. 253 (1975) 824.
[12] L.E. Alexander, X-ray Diffraction Methods in Polymer Science, Wiley, New York, 1969.
[13] D. Ferrer-Balas, M.L.L. Maspoch, A.B. Martinez, O.O. Santana, Influence of annealing on the microstructural, tensile and fracture properties of polypropylene films, Polymer 42 (2001) 1697.
[14] I.M. Ward, P.D. Coates, M.M. Dumoulin (Eds.), Solid Phase Processing of Polymers, Hanser, 2000.
[15] R.B. Bird, W.E. Stewart, E.N. Lightfoot, Transport Phenomena, 2nd ed., John Wiley & Sons Inc., 2001.